Chapter 8

The Sun: Life and Times on the Main Sequence

In the preceding chapter we considered the collapse of a protostar to the main sequence In this chapter we examine the nature of life on the main sequence for such a star.

- The essence of life on the main sequence is stable burning of H into He in hydrostatic equilibrium, by
  - PP chains for stars of a solar mass or less, and
  - the CNO cycle for more massive main-sequence stars.
- Since we have examined in some detail hydrostatic equilibrium, energy production by the PP chains and the CNO cycle, *we already understand the essence of life on the main sequence.*

It is appropriate that we begin by examining this main sequence star that we know the best: *the Sun.*

8.1 The Standard Solar Model

The Sun is by far the most studied star. We have a large amount of relevant data, and considerable understanding of how the Sun functions. This has allowed the construction of a *Standard Solar Model:*

> ***Standard Solar Model:*** a mathematical model of the Sun that uses
>
> - a basic understanding of such fields as nuclear and atomic physics,
> - measured key quantities, and
> - a few assumptions
>
> to describe all solar observations.

Standard Solar Models are important because

- They fix the Sun's *helium abundance*.
- They fix the Sun's *convection length scale* in the solar surface.
- They provide a *benchmark* for measuring improved solar modeling.
- They provide a *starting point* for more general stellar modeling.

The essence of the Standard Solar Model is that a *1 $M_\odot$ ZAMS star* is evolved to the present age of the Sun subject to the following assumptions:

1. The Sun was *formed from a homogeneous mixture* of gases.
2. The Sun is *powered by nuclear reactions* in its core.
3. The Sun is *approximately in hydrostatic equilibrium*, with the gravitational forces that attempt to compress it almost exactly compensated by forces arising from gradients in internal gas and radiation pressure.
4. *Some deviation from equilibrium* is permitted as the Sun evolves, but these are assumed to be *small and slow.*
5. Energy is transported from the core, where it is produced, to the surface, where it is radiated into space
   - by photons *(radiative transport)*
   - by large-scale vertical motion of packets of hot gas *(convection).*
   - The *role of conduction is considered negligible.*

Let us now discuss each of these assumptions that enter the Standard Solar Model in a little more depth.

8.1.1 Composition of the Sun

- The assumption that the Sun was formed from a *homogenous mixture of gases* is motivated by the *strong convection of the protostar* during collapse to the main sequence.
- The surface abundances are then assumed to have been undisturbed in the subsequent evolution, so that *present surface abundances are an accurate reflection of the composition of the original solar core.*
- *The abundance of most elements in the surface can be inferred by spectroscopy,* except for the noble gases He, Ne, and Ar. They are not excited significantly by the blackbody emission spectrum of the photosphere, so their abundance cannot be determined well from the spectrum.
- Because evolution of the Sun's luminosity depends on the mean molecular weight raised to the power 7.5 (see Exercise 8.1), which is strongly influenced by the helium abundance, *the H/He ratio is normally taken as an adjustable parameter in solar models.*
- The *H/He ratio* is determined by requiring that the luminosity of the Sun at the present age of the Solar System (4.6 billion years, as determined by dating meteorites) be accurately reproduced by the model.

8.1.2 Nuclear Energy Generation and Composition Changes

The Sun is assumed to derive its power and associated composition changes from

- the proton–proton chains PP-1, PP-2, and PP-III
- the CNO cycle.

The nuclear reaction networks describing this energy and element production are solved by

- dividing the Sun into concentric shells,
- calculating the nuclear reactions in each shell as a function of the current temperature and density there, and
- using the updated composition and the energy production as constant input to the partial differential equations describing the solar equilibrium structure.

8.1.3 Hydrostatic Equilibrium

Since the dynamical timescale of the Sun is less than an hour,

$$\tau_{\rm hydro} \simeq (G\bar{\rho})^{1/2} \simeq 55 \text{ minutes},$$

the Sun may be expected to have reached hydrostatic equilibrium quickly.

- However, a Standard Solar Model allows *small expansions and contractions* in response to time evolution of the star.
- *Re-equilibration is assumed to be very fast* compared with the timescale for evolution.
- The pressure is
  - composed of both gas pressure and radiation pressure, but
  - the radiation pressure even at the center is only about 0.05% of the total pressure.
- A Standard Solar Model typically *ignores the effects of both rotation and the part of the pressure deriving from magnetic fields* on hydrostatic equilibrium.
- Likewise, any *stellar pulsations are assumed to have negligible effect on hydrostatic equilibrium.*

8.1.4 Energy Transport

It is assumed that energy transport in the Sun by acoustic or gravitational waves is negligible, and that the energy produced internally in the Sun is transported by radiative diffusion and convection to the surface.

- In the interior, transport is assumed to be by radiative diffusion unless the critical gradient for convective instability is exceeded, in which case the Sun transports energy in that region convectively with an adiabatic temperature gradient
- In the surface region, the actual gradient is steeper than the adiabatic gradient and mixing length theory is used to model convection.
- Because convection in the surface region is difficult to calculate reliably, the mixing length in units of the *scale height is taken as an adjustable parameter,* to be fixed by requiring the model to yield the observed radius of the Sun.
- The opacities required for radiative diffusion of energy are Rosseland mean opacities that must be calculated numerically. They are among the *least well-determined quantities entering the Standard Solar Model,* with typical uncertainties in the 10–20% range.

Optical depth and the solar surface

The *optical depth* τ at radius r is defined in terms of the radiative opacity κ by

$$\tau = \int_r^\infty \kappa \rho \, dr.$$

It is dimensionless (κ has units of (length)^2/mass) and measures the *probability that photons interact with solar material before being radiated into space.*

- The radius of the Sun is defined to be that *distance from the center where the optical depth is* $\frac{2}{3}$.
- The diffusion approximation for radiative transport fails when τ is lower than about 1–10 because the mean free path for photons then becomes very long.

  In the solar surface, the photon mean free path is $\sim 10^7$ cm or longer, compared with fractions of a cm in the interior.

- The region of the solar surface where optical depth is less than about 1 is called the *solar atmosphere.*
- Radiative transport in the solar atmosphere is much more complicated than for the solar interior because *the diffusion approximation fails.*
- It is essential to model the atmosphere adequately because it *defines outer boundary conditions* and this is *where the solar spectrum is produced.*

8.1.5 Constraints and Solution

Solution of the Standard Solar Model problem corresponds to

- evolving in time four partial differential equations in five unknowns (P, T, r, $m(r)$, and L),
- supplemented by an equation of state and equations governing composition change (one for each species),
- subject to constraints on calculated radius, luminosity, and mass.

Two equations governing hydrostatic equilibrium,

$$\frac{dm}{dr} = 4\pi r^2 \rho(r) \qquad \text{Mass conservation}$$
$$\frac{dP}{dr} = -\frac{Gm(r)}{r^2}\rho \qquad \text{Hydrostatic equilibrium,}$$

three equations for luminosity and temperature gradients,

$$\frac{dL}{dr} = 4\pi r^2 \varepsilon(r) \qquad \text{Luminosity}$$
$$\frac{dT}{dr} = -\frac{3\rho(r)\kappa(r)}{4acT^3(r)}\frac{L(r)}{4\pi r^2} \qquad \text{(If radiative)}$$
$$\frac{dT}{dr} = \left(\frac{\gamma-1}{\gamma}\right)\frac{T}{P}\frac{dP}{dr} \qquad \text{(If convective),}$$

equations governing composition changes,

$$\frac{dn}{dt} = -\frac{1}{\tau}n \qquad \text{Nucleosynthesis,}$$

and an equation of state,

$$P = P(T, \rho, X_i, \ldots) \qquad \text{Equation of state.}$$

The network of equations required to describe nuclear energy and element production is solved separately for each timestep in each zone.

- The equation of state is assumed to be given by the ideal gas law for regions that are completely ionized.
- Otherwise, a numerical equation of state calculated at Lawrence Livermore National Laboratory is typically used.
- The Standard Solar Model solution is constructed iteratively.
- Starting values for the
  - *helium abundance* and the
  - *mixing length* parameter

  are used to evolve an initial zero-age model to the current age of the Sun.
- The model's
  - *luminosity* and
  - *radius*

  are then compared with observations, the helium abundance and mixing length parameters adjusted accordingly, and the model is evolved again.
- This cycle is repeated until convergence is obtained.

Table 8.1 gives the temperature, density, pressure, and luminosity of a Standard Solar Model as a function of radius and enclosed mass at that radius.

Table 8.1: A Standard Solar Model

$M/M_\odot$	$R/R_\odot$	T(K)	ρ (g cm^{-3})	P (dyn cm^{-2})	$L/L_\odot$
0.0000298	0.00650	1.568E+07	1.524E+02	2.336E+17	0.00027
0.0008590	0.02005	1.556E+07	1.483E+02	2.280E+17	0.00753
0.0065163	0.04010	1.516E+07	1.359E+02	2.111E+17	0.05389
0.0207399	0.06061	1.456E+07	1.193E+02	1.868E+17	0.15638
0.0439908	0.08041	1.386E+07	1.027E+02	1.606E+17	0.29634
0.0762478	0.10006	1.310E+07	8.729E+01	1.349E+17	0.45135
0.1173929	0.12000	1.231E+07	7.350E+01	1.108E+17	0.60142
0.1672004	0.14056	1.150E+07	6.123E+01	8.892E+16	0.73152
0.2203236	0.16027	1.076E+07	5.114E+01	7.094E+16	0.82657
0.2800107	0.18104	1.002E+07	4.205E+01	5.517E+16	0.89658
0.3393826	0.20107	9.353E+06	3.459E+01	4.279E+16	0.94011
0.3966733	0.22038	8.762E+06	2.847E+01	3.319E+16	0.96616
0.4559683	0.24084	8.188E+06	2.301E+01	2.516E+16	0.98259
0.5114049	0.26085	7.676E+06	1.857E+01	1.907E+16	0.99183
0.5627338	0.28058	7.214E+06	1.496E+01	1.446E+16	0.99669
0.6099028	0.30016	6.794E+06	1.203E+01	1.096E+16	0.99860
0.6564038	0.32132	6.379E+06	9.484E+00	8.119E+15	0.99941
0.6952616	0.34091	6.028E+06	7.605E+00	6.156E+15	0.99976
0.7304369	0.36063	5.703E+06	6.092E+00	4.667E+15	0.99993
0.7621708	0.38053	5.400E+06	4.876E+00	3.539E+15	1.00002
0.7907148	0.40067	5.117E+06	3.900E+00	2.683E+15	1.00005
0.8163208	0.42109	4.851E+06	3.118E+00	2.034E+15	1.00007
0.8374222	0.44008	4.621E+06	2.539E+00	1.578E+15	1.00007
0.8580756	0.46112	4.383E+06	2.029E+00	1.197E+15	1.00006
0.8750244	0.48072	4.176E+06	1.651E+00	9.287E+14	1.00006
0.8902432	0.50063	3.978E+06	1.345E+00	7.206E+14	1.00005
0.9038831	0.52086	3.789E+06	1.095E+00	5.591E+14	1.00004
0.9160850	0.54139	3.606E+06	8.924E-01	4.339E+14	1.00004
0.9260393	0.56033	3.445E+06	7.413E-01	3.445E+14	1.00003
0.9358483	0.58142	3.273E+06	6.052E-01	2.673E+14	1.00003

Table 8.1: (Continued) Standard Solar Model

$M/M_\odot$	$R/R_\odot$	T(K)	ρ (g cm^{-3})	P (dyn cm^{-2})	$L/L_\odot$
0.9438189	0.60081	3.120E+06	5.040E-01	2.123E+14	1.00002
0.9509668	0.62036	2.969E+06	4.205E-01	1.686E+14	1.00002
0.9573622	0.64001	2.818E+06	3.517E-01	1.339E+14	1.00002
0.9636045	0.66168	2.648E+06	2.900E-01	1.039E+14	1.00001
0.9686223	0.68129	2.485E+06	2.445E-01	8.249E+13	1.00001
0.9730081	0.70042	2.315E+06	2.081E-01	6.572E+13	1.00001
0.9771199	0.72033	2.115E+06	1.780E-01	5.161E+13	1.00001
0.9811002	0.74162	1.899E+06	1.513E-01	3.936E+13	1.00000
0.9842836	0.76050	1.718E+06	1.299E-01	3.055E+13	1.00000
0.9874435	0.78148	1.526E+06	1.085E-01	2.264E+13	1.00000
0.9900343	0.80103	1.355E+06	9.066E-02	1.678E+13	1.00000
0.9922832	0.82051	1.193E+06	7.470E-02	1.215E+13	1.00000
0.9942853	0.84082	1.031E+06	5.987E-02	8.406E+12	1.00000
0.9958822	0.86022	8.826E+05	4.733E-02	5.682E+12	1.00000
0.9972278	0.88035	7.356E+05	3.590E-02	3.585E+12	1.00000
0.9982619	0.90020	5.966E+05	2.613E-02	2.110E+12	1.00000
0.9990296	0.92017	4.627E+05	1.775E-02	1.107E+12	1.00000
0.9995498	0.94015	3.343E+05	1.080E-02	4.833E+11	1.00000

$M_\odot = 1.989 \times 10^{33}$ g $\quad R_\odot = 6.96 \times 10^{10}$ cm $\quad L_\odot = 3.827 \times 10^{33}$ erg s^{-1}

Figure 8.1 illustrates graphically some of the parameters of this model plotted versus the radius and Fig. 8.2 plots the same quantities versus the enclosed mass coordinate.

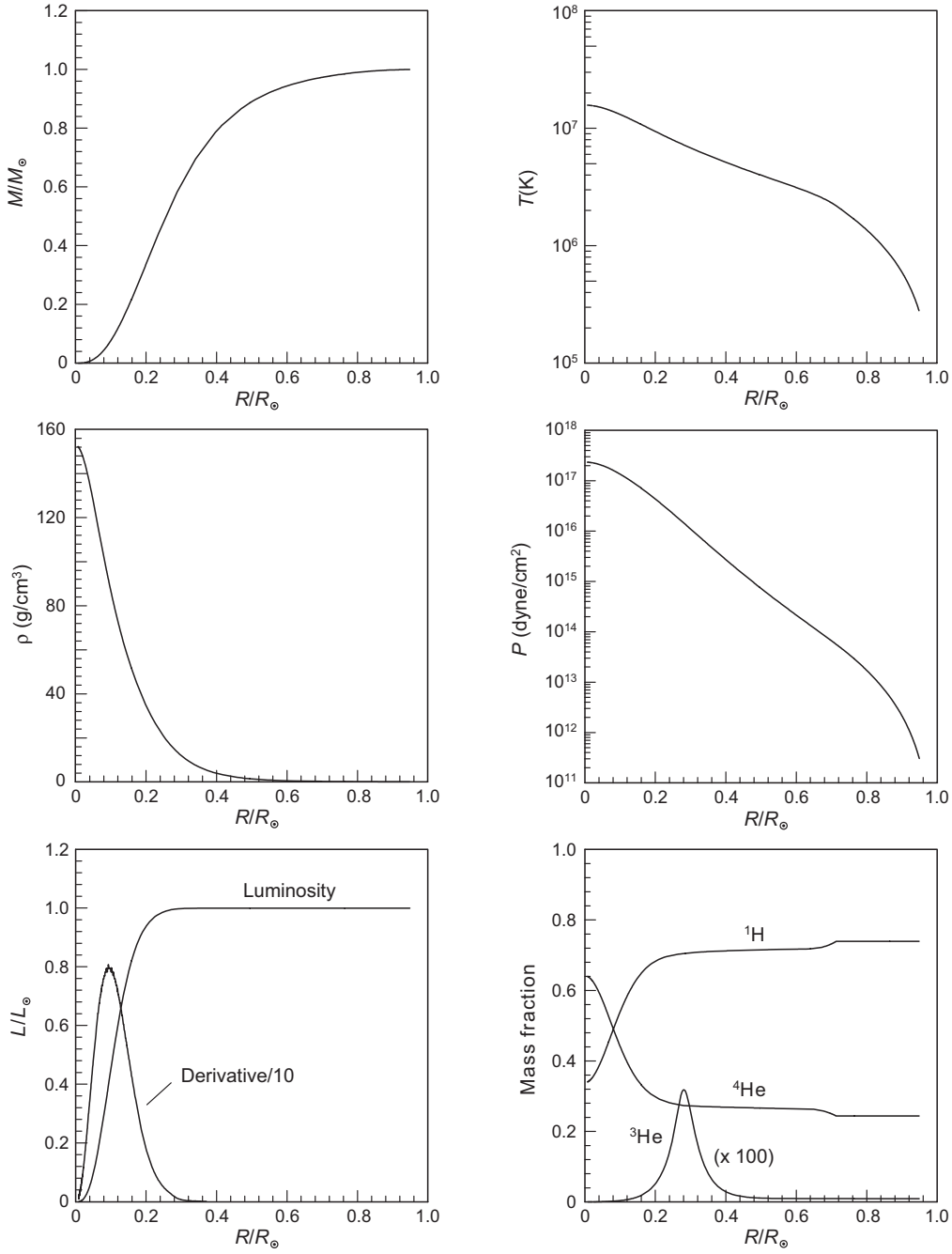

Figure 8.1: Parameters from a Standard Solar Model (Table 8.1) plotted versus the radial coordinate.

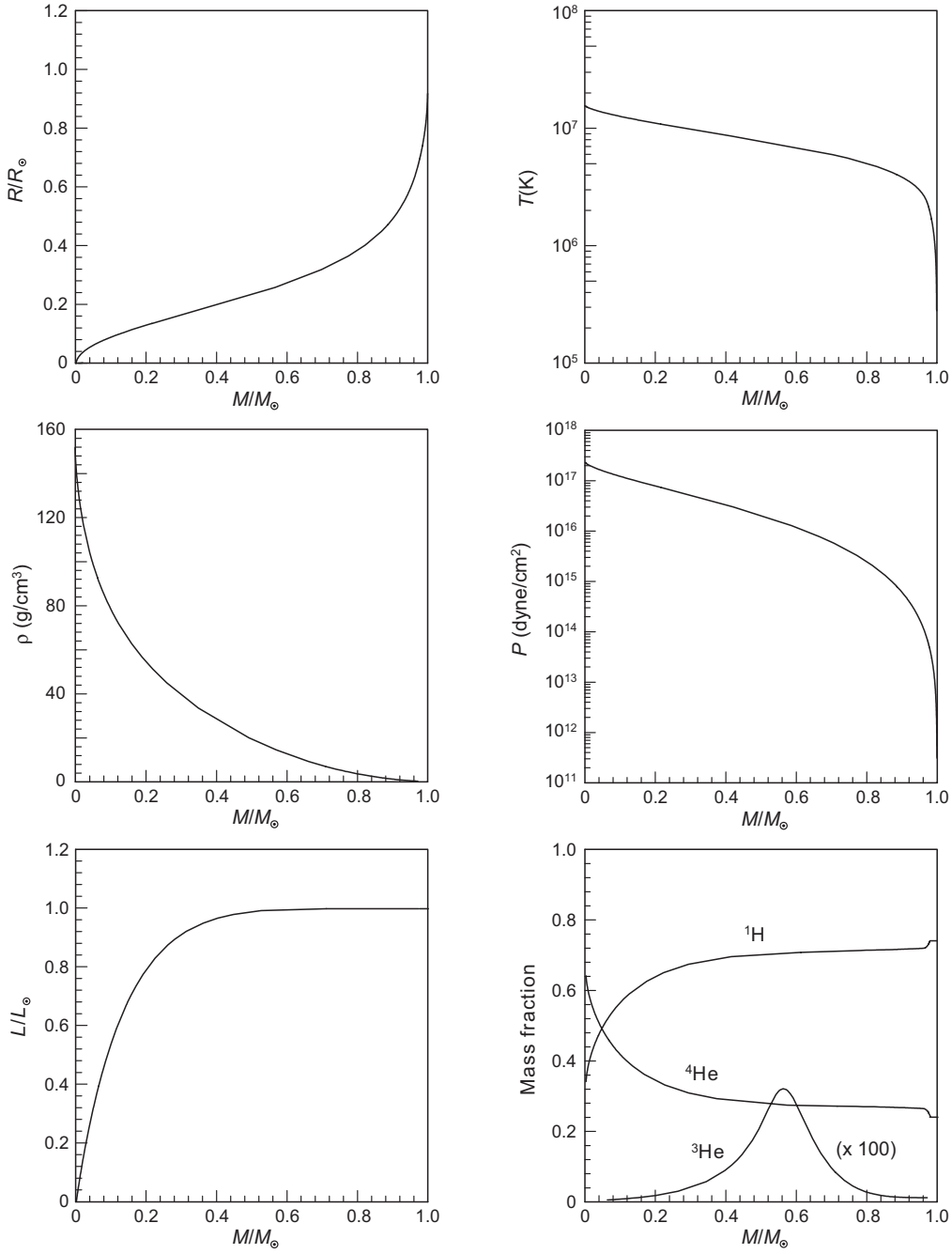

Figure 8.2: Parameters from a Standard Solar Model (Table 8.1) plotted versus the enclosed mass.

The Standard Solar Model may be tested by comparing its predictions with observations.

- These tests range from general ones, such as *accounting for the existence, age, and energy output* of the Sun, to specific ones such as the *accounting for the results of solar seismology.*
- Generally, the Standard Solar Model has passed these tests very well.

We now discuss two examples of how the Standard Solar Model description of the solar interior can be tested:

- the subsurface structure as inferred from *helioseismology* and
- the spectrum and overall *flux of neutrinos* emitted from the solar core.

8.2 Helioseismology

One way to study the Sun's interior is to study the propagation of waves in its body.

- This is similar to the way geologists learn about the interior of the Earth by studying seismic waves.
- The corresponding field of study is called *helioseismology.*

8.2.1 p-Modes

Solar oscillations were discovered by studying Doppler shifts of surface absorption lines.

- It was found that the solar surface consists of patches oscillating on a timescale of five minutes with a velocity amplitude of 0.5 km s^{-1}.
- These 5-minute oscillations represent pressure waves (*p-modes*) trapped between the surface and the lower boundary of the convective zone.
  - They are *reflected from the solar surface* by density gradients.
  - They are *refracted near the bottom of the convection zone* because of changing soundspeed in that region.

8.2.2 g-Modes

In addition to p-modes associated with acoustical waves trapped near the solar surface, the Sun may also exhibit *g-modes:*

- These correspond to oscillations in which the *restoring force is gravity.*
- If g-modes can be observed, they *carry information about much deeper regions of the Sun* than that carried by the p-modes.

8.2.3 Surface Vibrations and the Solar Interior

One can learn about waves in the interior by dividing the surface of the Sun up into small regions and determining the radial velocity of each region from Doppler shifts.

- The result is called the *velocity field* for the Sun.
- A diagram showing how the velocity field varies across the solar disk is called a *dopplergram.*
- Superposed on the overall rotational motion are fluctuations corresponding to vertical motion of the Sun's surface in localized regions.
- The Michelson Doppler Imager (MDI) instrument on the SOHO observatory is orbiting the Sun 1.5 million kilometers sunward from the Earth.
- It is capable of measuring vertical displacement on the solar surface at a million points simultaneously and can detect displacement velocities as small as $1\ \mathrm{mm\,s^{-1}}$.

The Sun vibrates at a complex set of frequencies, with the dominant frequency corresponding to the 5-minute oscillation described above.

- By decomposing the observed vibration of the Sun into a superposition of standing acoustic waves, it is possible to learn about the interior.
- Such decompositions indicate that the observed motion of the surface is a superposition of several million resonant modes with different frequencies and horizontal wavelengths.
- Individual modes in this decomposition may have velocity amplitudes as large as 20 $\mathrm{cm\,s^{-1}}$ and 1–2 meter vertical displacements.

Presently, helioseismology is placing strong constraints on our theories of the solar interior.

- The analysis is complex but the basic idea is simple: *changes in the properties of the solar interior (for example, the amount of helium in some region) affects the way sound waves travel through the interior.*
- This will in turn influence the way the surface vibrates.

Two important pieces of information obtained from early helioseismology are that

- the abundance of helium in the interior (but outside the core) is about the same as at the surface,
- convection extends about 30 percent of the way to the center.

We discuss in the next two sections information from helioseismology concerning sound speed in the solar interior and the rotation of the solar interior.

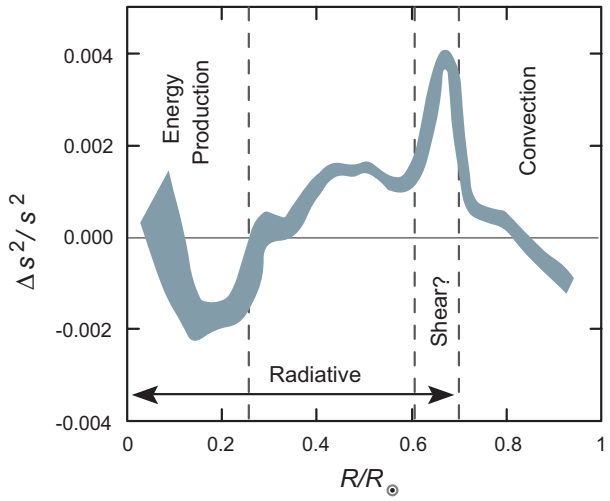

Figure 8.3: Deviation of the sound speed inferred using helioseismology from that predicted by the Standard Solar Model.

8.2.4 Speed of Sound in the Sun

The speed of sound is sensitive to internal properties.

- Figure 8.3 illustrates information about the speed of sound inside the Sun as inferred from SOHO helioseismology.
- The data are shown in the form of the fractional deviation of the square of the sound speed s from that expected from the Standard Solar Model, with zero indicating perfect agreement.
- The finite extent of the shaded area indicates the uncertainty in the measurement.

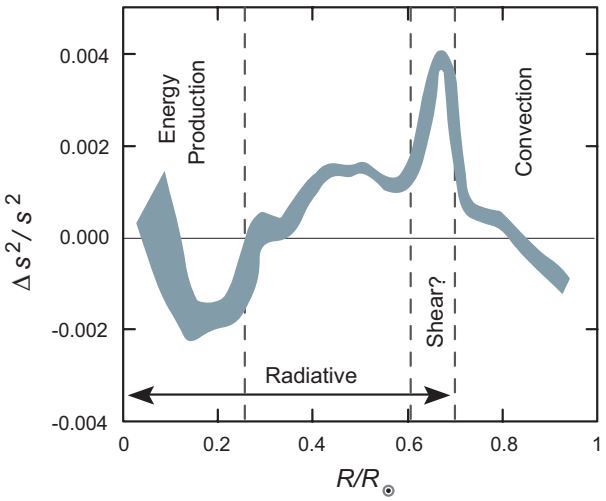

- The deviations are very small (fraction of a percent).
- Largest deviations are concentrated in two regions:
  - a region just below the convection boundary at about 60–70 percent of the solar radius and
  - a region in the energy-producing zone near about 20 percent of the solar radius.
- Both deviations are thought to result from *small differences in helium concentration* from that predicted by the accepted models of the Sun.
- Negative deviations imply higher helium concentration; positive imply reduced helium concentration.

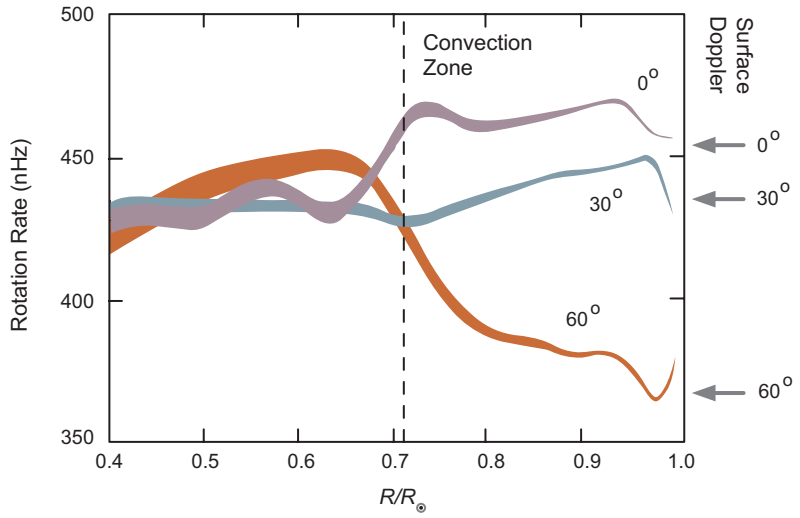

Figure 8.4: Rotation rates at different latitudes in the Sun as a function of radius, as inferred from helioseismology with SOHO. Near the surface the rotation rate is different at different latitudes but inside the convection zone the rotation rates at all latitudes become similar.

8.2.5 Internal Rotation Rate of the Sun

Data from SOHO helioseismology have also been used to deduce the internal rotation rate of the Sun. Figure 8.4 illustrates rotation rates inferred from solar vibrational data.

- Results are plotted for three different latitudes versus the fraction of the solar radius; widths of the curves indicate the estimated uncertainties in the measurements.
- The surface velocities at these latitudes as measured directly by Doppler shifts are indicated by the arrows on the right side.
- We notice the *differential rotation* near the surface (different latitudes rotating at different rates), as was already known from surface observations.

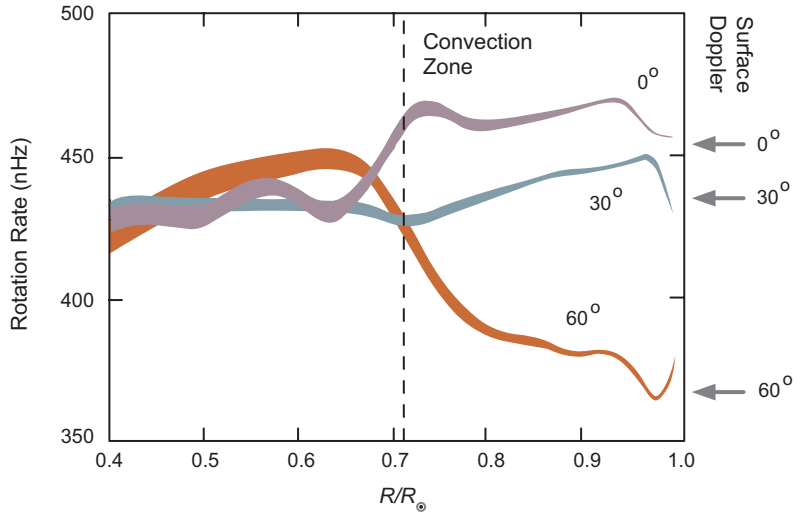

- But the helioseismology data indicate that inside the convective zone, beginning at about 65 percent of the solar radius, the Sun begins to rotate almost as a rigid body.
- That is, the curves for the three different latitudes converge to similar values, indicating that all latitudes are rotating with about the same rate.

8.3 Solar Neutrino Production

Helioseismology allows us to probe the interior of the Sun. A second way in which we can study the (deep) interior of the Sun is by detecting the neutrinos that are produced there.

- The energy powering the surface photon luminosity must make its way on a 100,000-year or greater timescale to the surface before being radiated.
- Neutrinos emitted from the core are largely unimpeded in their exit from the Sun, reaching the Earth 8.5 minutes after they were produced.

Therefore, neutrinos carry *immediate and more direct information* about the current conditions in the solar core than do the photons emitted from the solar photosphere.

- There are eight reactions or decays that are of some significance in solar energy production that may produce neutrinos:

pp	$p + p \rightarrow {}^2H + e^+ + \nu_e$	$Q \leq 0.420$ MeV
pep	$p + e^- + p \rightarrow {}^2H + \nu_e$	$Q = 1.442$ MeV
hep	${}^3He + p \rightarrow {}^4He + \nu_e$	$Q \leq 18.773$ MeV
${}^7Be$	${}^7Be + e^- \rightarrow {}^7Li + \nu_e$	$Q = 0.862$ MeV (89.7%)
		$Q = 0.384$ MeV (10.3%)
${}^8B$	${}^8B \rightarrow {}^8Be^* + e^+ + \nu_e$	$Q \leq 15$ MeV
CNO	${}^{13}N \rightarrow {}^{13}C + e^+ + \nu_e$	$Q \leq 1.199$ MeV
CNO	${}^{15}O \rightarrow {}^{15}N + e^+ + \nu_e$	$Q \leq 1.732$ MeV
CNO	${}^{17}F \rightarrow {}^{17}O + e^+ + \nu_e$	$Q \leq 1.740$ MeV

- Six of the reactions produce spectra with a range of Q-values and two are line sources.
- Neutrinos from the CNO reactions are difficult to detect because
  - they are weak (less than 2% of the Sun's energy comes from the CNO cycle)
  - the energies are low.
- Therefore, our primary concern will be with the first five reactions, which correspond to steps of the PP chains.
- The solar neutrino spectrum predicted by the Standard Solar Model is shown in Fig. 8.5 and Fig. 8.6 illustrates the radial regions of the Sun responsible for producing neutrinos from each of the PP reactions.

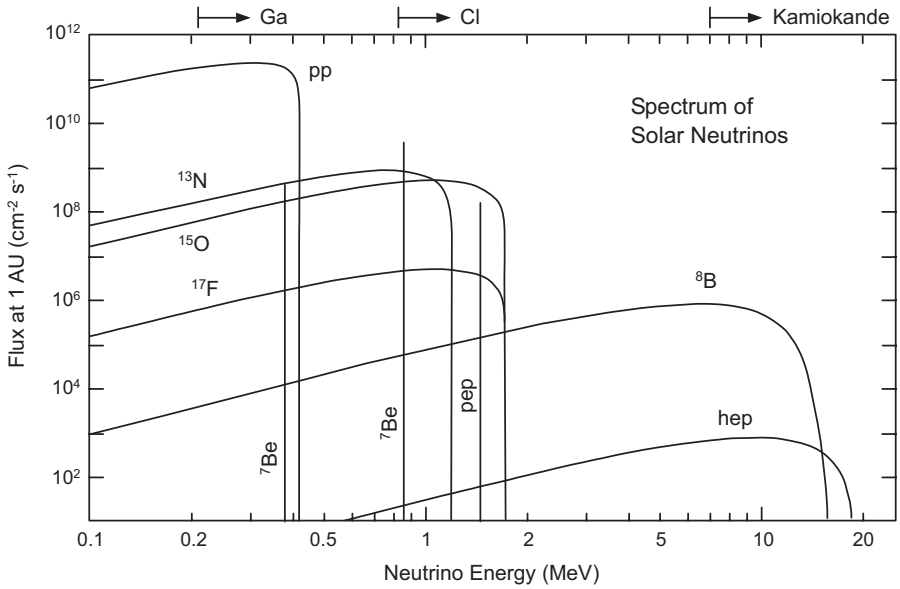

Figure 8.5: The solar neutrino spectrum. The sensitive region of various experiments is indicated above the graph.

The solar neutrino spectrum predicted by the Standard Solar Model is shown in Fig. 8.5.

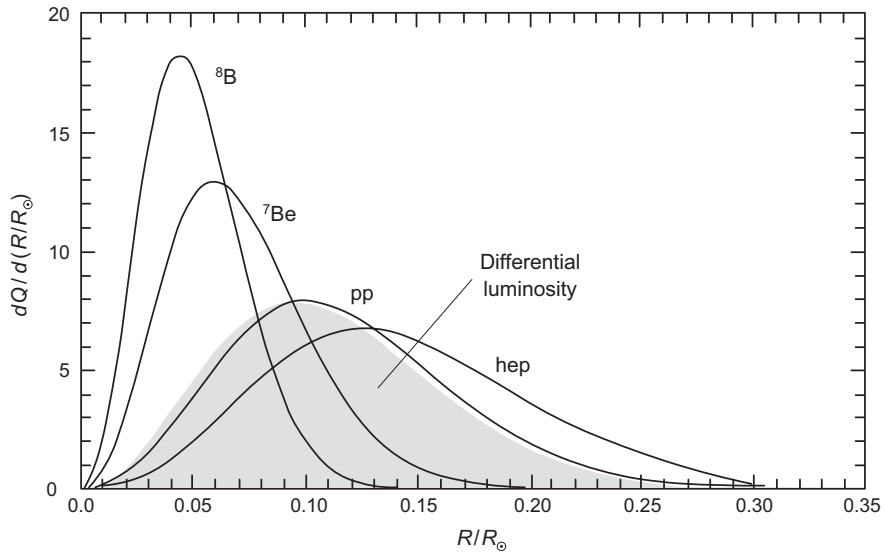

Figure 8.6: Differential neutrino production as a function of solar radius. The shaded area indicates the differential photon luminosity.

Fig. 8.6 illustrates the radial regions of the Sun responsible for producing neutrinos from each of the PP reactions.

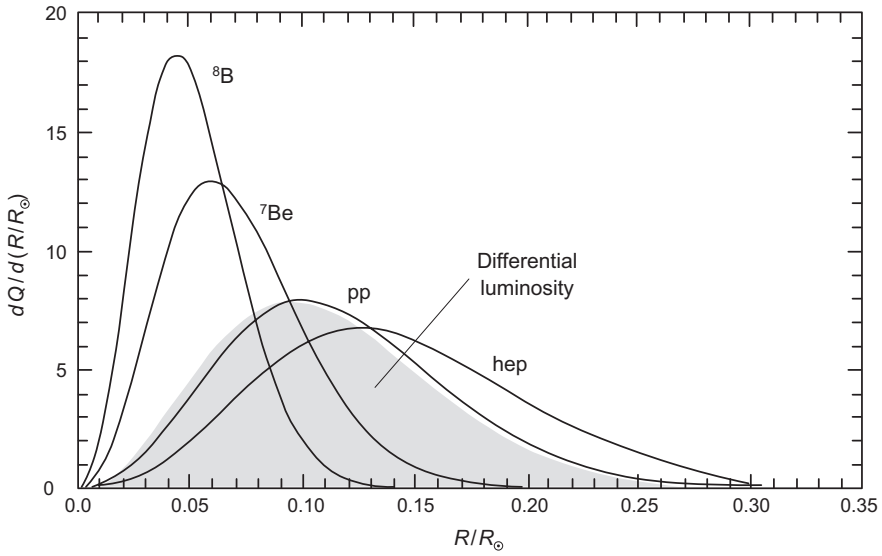

- Notice from the above figure that the ^{8}B and ^{7}Be neutrinos probe much smaller radii than the photons or neutrinos produced in PP-I (labeled pp), because they are produced at higher temperatures.
- Attempts to understand the observed rate of neutrino emission from the Sun yielded initially surprising results suggesting that our fundamental understanding of either (or both) elementary particle physics and the way the Sun works were incomplete.
- Resolution of this issue has led to profound new understanding in both astrophysics and elementary particle physics.

8.4 Solar Neutrinos

In the preceding sections we discussed the internal structure of the Sun and suggested that neutrinos emitted by thermonuclear processes in the central region of the Sun carry direct information about the state of the core.

- In this and following sections we elaborate on the physics of solar neutrinos.
- Reconciliation of solar neutrino observations with our understanding of elementary particle physics has had fundamental implications both for astrophysics and for elementary particle physics.

Although our discussion will involve directly only the Sun because it is the only star near enough to allow its emitted neutrinos to be detected on Earth with present technology, presumably the physics described in this chapter also operates in other stars.

8.5 Evolutionary Timescales

A question of basic importance is how long a star will remain on the main sequence.

- Evolution prior to the main sequence is governed by two primary timescales:
  1. The *hydrodynamical (free-fall) timescale*
  2. The *Kelvin–Helmholtz (thermal adjustment) timescale.*
- Evolution on the main sequence and beyond is governed in addition by a third timescale, the *nuclear burning timescale.*
- The hydrodynamical timescale is typically hours to days for most stars.
- The Kelvin–Helmholtz timescale is typically hundreds of thousands to hundreds of millions of years.
- The nuclear burning timescale depends on the fuel being burned and the mass of the star (among other factors), but is typically much longer than the hydrodynamic and Kelvin–Helmholtz timescales.
- Thus, stars spend much more time on the main sequence than in their formation phase because time spent on the main sequence is governed by the hydrogen burning timescale, which is much longer than the hydrodynamical and Kelvin–Helmholtz timescales.

For the Sun

- the *hydrodynamical timescale* is about *1 hour,*
- the *Kelvin–Helmholtz timescale* is about *10 million years*, and
- the *nuclear timescale* (time to burn the core hydrogen fuel on the main sequence) is about *10 billion years.*

Once stars exhaust their core hydrogen and leave the main sequence, they can undergo successive burnings of heavier fuels, which introduce new nuclear burning timescales.

- In the periods between exhaustion of one fuel and ignition of another, thermal adjustment timescales will also be important.
- In certain cases (such as gravitational core collapse) hydrodynamical timescales will be relevant.
- The nuclear burning timescales that become important after the main sequence are typically longer than the corresponding Kelvin–Helmholtz and hydrodynamical timescales, just as for the main sequence.
- However, post main-sequence burning timescales are much shorter than that for main-sequence hydrogen burning because they necessarily occur at much higher temperatures and densities.
- Thus, a star generally spends more time on the main sequence than in its post main-sequence evolution.
- We conclude that the nuclear burning timescale on the main sequence is longer than any timescale in any other stage of the star's life.
- Thus at any one time in a population of stars we expect to see the majority on the main sequence (unless the age is sufficiently large that most stars have had time to evolve off the main sequence).

8.6 Evolution of Stars on the Main Sequence

The main sequence is the longest and most stable period of a star's life but stars do evolve on the main sequence, primarily in response to core concentration changes as they burn hydrogen to helium in hydrostatic equilibrium.

- This *lowers the pressure in the core* because it increases the mean molecular weight μ:

$$P = \rho \frac{kT}{\mu}$$

- This in turn *increases the core density and releases gravitational energy,* half of which is radiated away and half of which raises the core temperature (the *virial theorem*).
- Because of the higher core temperature
  - the energy outflow causes *the outer layers to expand* slightly and
  - *the star becomes more luminous* in response to the core increase in temperature.
- Dependence of luminosity on the mean molecular weight is strong, varying as approximately the 7.5 power of the mean molecular weight (Exercise 8.1).

- The surface temperature during evolution on the main sequence may either increase or decrease.
  - For stars below about 1.25 $M_\odot$ the surface temperature tends to increase.
  - For more massive stars it tends to decrease as the star evolves on the main sequence.
- Therefore, the primary external effect of a star's evolution on the main sequence is to cause a small drift from the ZAMS position in the HR diagram:
  - Slightly upward and to the left for lighter stars.
  - Slightly upward and to the right for heavier stars.
- Internally the changes are more substantial, but their effects are often not very visible externally while the star continues to burn core hydrogen.
- Significant modification of elemental abundances is taking place as a result of the core fusion, but these changes are limited initially to the central regions.

The Standard Solar Model indicates that over the 4.6 billion year time that the Sun has spent on the main sequence

- The radius has increased by about 12%,
- The core temperature has increased by about 16%,
- The luminosity has increased by about 40%,
- The effective surface temperature has increased by about 3%, and the flux of ^{8}B neutrinos has increased by more than a factor of 40.
- Near the center the mass fraction of hydrogen has decreased and the mass fraction of helium has increased by about a factor of 2 from their initial values,
- Outside of about 20% of the solar radius hydrogen and helium retain their ZAMS abundances.
- The mass fraction of hydrogen fuel has decreased substantially in the solar core over its lifetime, but the rate of energy production by the PP chain is

$$\frac{d\varepsilon}{dt} \simeq \rho^2 X^2 T^4,$$

where ρ is the density, X the hydrogen mass fraction, and T the temperature.

  - Increasing ρ and T more than offset decreasing X as the Sun evolves on the main sequence.
  - This explains why the Sun's luminosity is rising even as its hydrogen fuel is being depleted.

Although the internal changes discussed in the preceding example lead to only small visible external modification of the star on the main sequence, they set the stage for rapid evolution away from the main sequence that will be the topic of subsequent chapters.

8.7 The Solar Electron-Neutrino Deficit

By counting the number of neutrinos produced and the average energy released for each $4\mathrm{H} \rightarrow {}^{4}\mathrm{He}$ in the PP chains, we may estimate that

- The Sun should be emitting approximately 10^{38} *electron neutrinos per second* if it is powered by the PP chains (see Exercise 8.4).
- However, detectors on Earth see only a fraction of the corresponding number of electron neutrinos that should reach Earth. This has historically been termed the *solar neutrino problem.*

That there is a problem is confirmed by the solar neutrino experiments described in the following subsections.

8.7.1 The Davis Chlorine Experiment

The pioneering solar neutrino detection experiment was started by Raymond Davis in the early 1960s.

- It used the reaction

$$\nu + {}^{37}\mathrm{Cl} \rightarrow {}^{37}\mathrm{Ar} + e^{-}$$

  initiated in 600 tons of cleaning fluid (C_2Cl_4).

- To shield against cosmic rays, the tank containing the cleaning fluid was placed 1500 meters below the surface in the abandoned Homestake gold mine in South Dakota.

- The small number of argon atoms produced by the above reaction are radioactive.

- Their decays can be counted after separation of the argon from the cleaning fluid by chemical means.

- The reaction $\nu + {}^{37}\mathrm{Cl} \rightarrow {}^{37}\mathrm{Ar} + e^{-}$ has a threshold (minimum energy for the reaction to occur) of 0.8 MeV, which is higher than the maximum energy of 0.42 MeV for neutrinos in the PP-I chain:

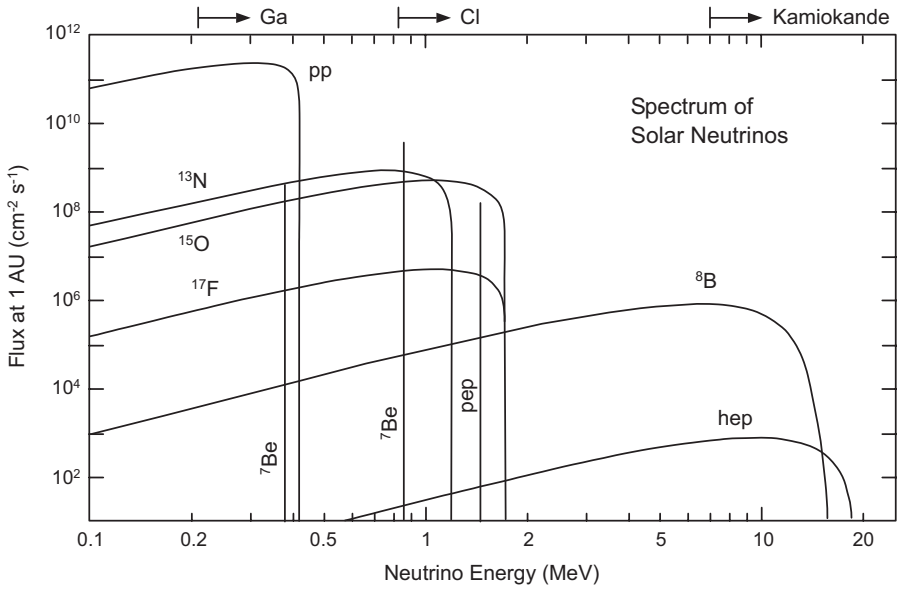

- Therefore, the Davis experiment was sensitive primarily to the ^{8}B neutrinos (and weakly to the ^{7}Be neutrinos).

> *The Davis experiment consistently counted neutrinos at a rate that was 2–3 times smaller than the rate predicted by the Standard Solar Model.*

- Because this detector is based on chemistry conducted after the reaction, it has *no directional sensitivity.*

8.7.2 The Gallium Experiments

The chlorine experiment is primarily sensitive to the ^{8}B neutrinos. These neutrinos probe the deepest regions of the Sun:

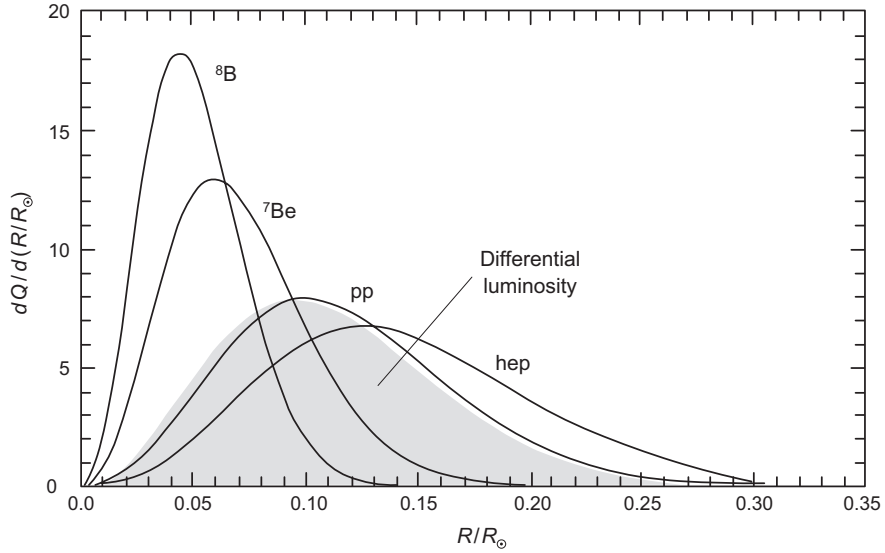

but they come come from a very minor side branch of PP

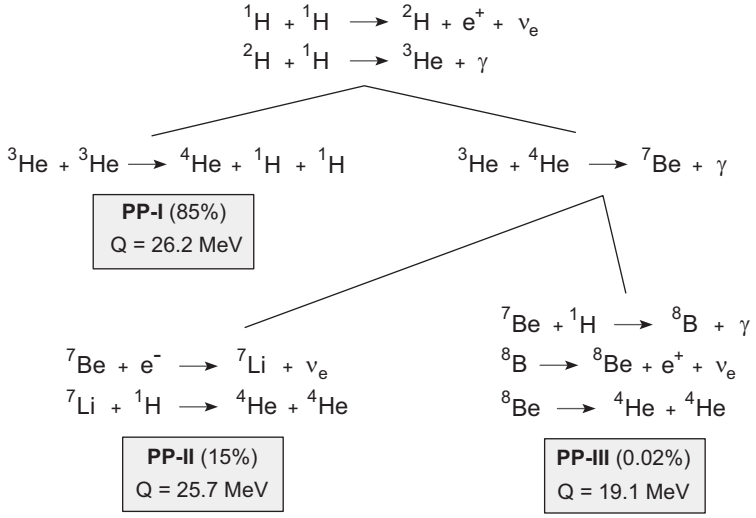

and thus are not very closely related to the Sun's photon luminosity.

Because of the threshold for the reaction $\nu + {}^{37}\mathrm{Cl} \rightarrow {}^{37}\mathrm{Ar} + e^{-}$ the neutrinos from the primary energy production process in the Sun (PP-I) are not detected at all.

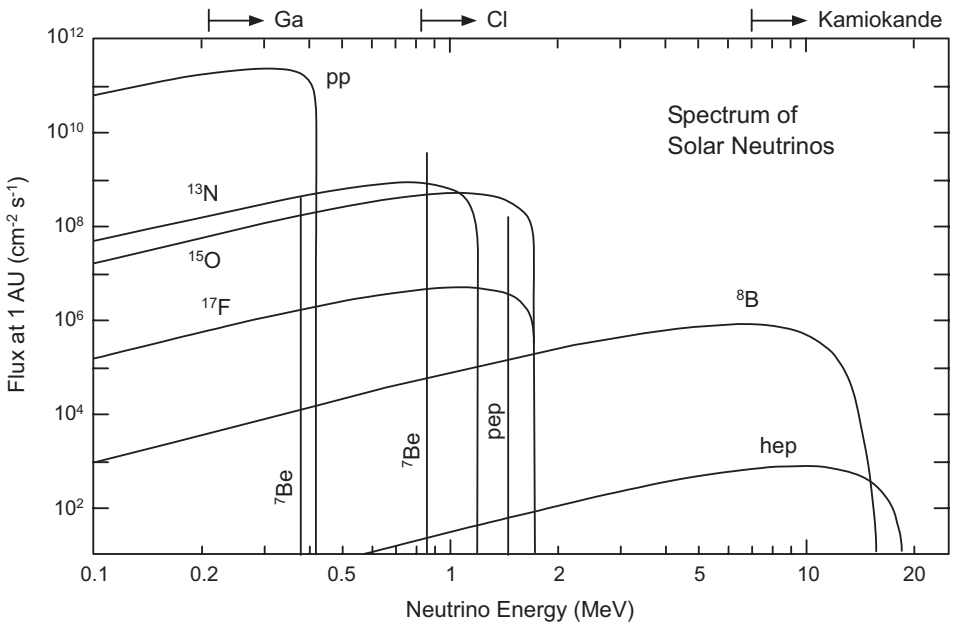

Another chemistry-based detection system can be constructed using the reaction

$$\nu + {}^{71}\mathrm{Ga} \rightarrow {}^{71}\mathrm{Ge} + e^{-}.$$

- The ${}^{71}\mathrm{Ge}$ produced is radioactive so the Ge can be separated chemically and its decay detected to count the number of neutrino reactions.
- The reaction $\nu + {}^{71}\mathrm{Ga} \rightarrow {}^{71}\mathrm{Ge} + e^{-}$ has a *threshold of only 0.23 MeV,* so it can detect neutrinos coming from the PP-I chain that produces most of the solar energy.

Two large experiments,

- *SAGE* (operated by a Russian–American collaboration underground in the Caucasus) and
- *GALLEX* (operated by a largely European collaboration in the Gran Sasso underground laboratory in Italy),

were implemented based on the gallium reaction $\nu + {}^{71}\mathrm{Ga} \rightarrow {}^{71}\mathrm{Ge} + e^{-}$.

- These experiments, for which more than half of the neutrinos are expected to come from the pp reaction in PP-I, *also measured a neutrino deficit compared with the Standard Solar Model.*
  - However, the deficit is not as large as in the chlorine experiment.
  - They found that the electron neutrino flux is reduced by a factor of about two relative to that expected.
- Like the chlorine experiment, the gallium experiments are chemistry-based and have *no directional sensitivity.*

8.7.3 Super Kamiokande

The Super Kamiokande detector *(Super-K)* operates in the Kamioka mine in Japan and uses a different approach to detecting neutrinos.

- A large tank containing 50,000 cubic meters of *ultrapure water* is monitored by photodetectors.
- When the elastic scattering reaction

$$\nu + e^- \rightarrow \nu + e^-$$

  occurs in the water, recoiling electrons may exceed the speed of light in the medium and produce *Čerenkov radiation* that is detected by the phototubes.
- The threshold for reliable detection in Super Kamiokande is about 7 MeV, so this detector is sensitive only to the *more energetic ^8B neutrinos produced in PP-III*

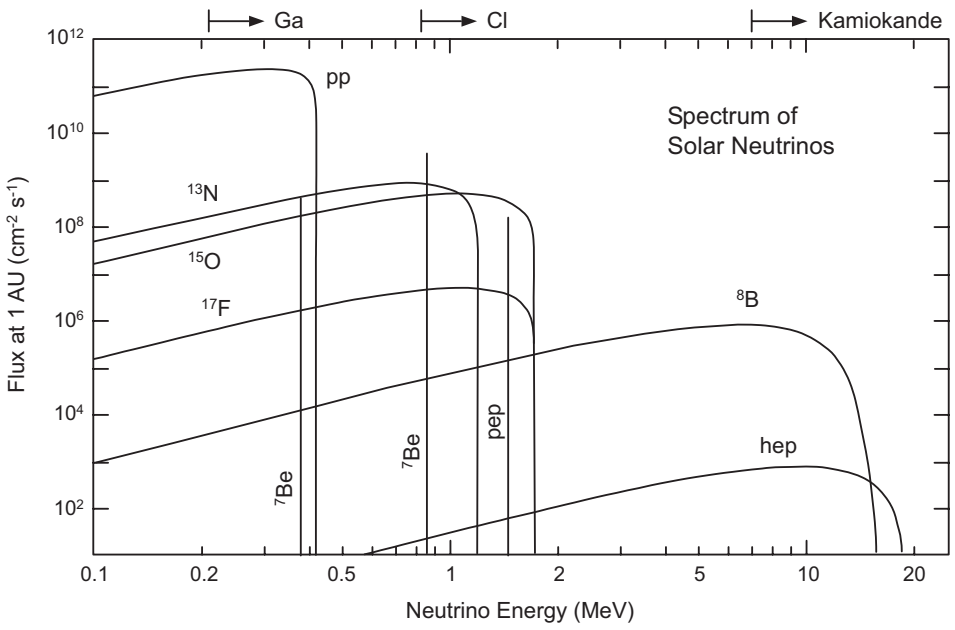

- Because the detector has *directional sensitivity,* Super Kamiokande (unlike the Davis experiment, Sage, or Gallex) is able to demonstrate that *the detected neutrinos come from the direction of the Sun.*
- The Super Kamiokande results again indicate a *solar neutrino deficit,* with the detector seeing fewer than 40% of the electron neutrinos expected based on fluxes predicted by the Standard Solar Model.

Table 8.2: Solar neutrino fluxes from various experiments compared with a Standard Solar Model (SSM). All fluxes are in solar neutrino units (SNU), except the result from Super Kamiokande. Experimental uncertainties include systematic and statistical contributions.

Experiment	Observed flux	SSM	Observed/SSM
Homestake	$2.54 \pm 0.14 \pm 0.14$ SNU	$9.3\ ^{+1.2}_{-1.4}$	0.273 ± 0.021
SAGE	$72\ ^{+12}_{-10}\ ^{+5}_{-7}$ SNU	$137\ ^{+8}_{-7}$	0.526 ± 0.089
GALLEX	$69.7 \pm 6.7\ ^{+3.9}_{-4.5}$ SNU	$137\ ^{+8}_{-7}$	0.509 ± 0.089
Super-Kamiokande	$2.51\ ^{+0.14}_{-0.13}$ $(10^6$ cm^{-2}s$^{-1})$	$6.62\ ^{+0.93}_{-1.12}$	0.379 ± 0.034

The experiments described above were not all sensitive to the same neutrinos from the Sun and found somewhat different magnitudes for the solar neutrino deficit.

- However, the chlorine experiment, the two gallium experiments, and the water Čerenkov detectors all find reproducibly that significantly fewer neutrinos are being detected coming from the Sun than the Standard Solar Model predicts.
- Table 8.2 summarizes and compares with the predictions of a Standard Solar Model.
- These results indicate a deficit of solar neutrinos in the detectors, and that the amount of the deficit depends on which neutrinos are being detected.
- Example: suppression of ^{8}B neutrinos appears to be larger than for the PP-I neutrinos, and data are consistent with essentially no ^{7}Be neutrinos being detected.

8.7.4 Astrophysics Versus Particle Physics Explanations

Confirmation in more recent experiments of the solar neutrino problem discovered by Davis implies two alternatives:

- We do not understand how the Sun works *(failure of the Standard Solar Model).*
- We do not understand the neutrino *(failure of the Standard Model of elementary particle physics).*

Thus, a debate ensued over whether the solution to the solar neutrino problem lay in a modification of our astrophysics understanding or of our particle physics understanding.

- Experiments and observations have shown rather conclusively that the "solar neutrino problem" is now resolved, and that *the resolution lies in new properties for neutrinos* that imply physics beyond the Standard Model of elementary particle physics.
- Specifically, we now have strong evidence that *at least some neutrinos have a non-zero mass,* and that this permits neutrinos to change their types from electron neutrinos (to which the above detectors are sensitive) into other types that the detectors described above cannot see.

To understand these *neutrino oscillations,* we must first understand weak interactions in the Standard Model of elementary particle physics and their properties in conjectured extensions of that model.

8.8 Weak Interactions and Neutrino Physics

The *Standard Model* of elementary particle physics assumes that the electromagnetic and weak interactions are unified in a local gauge or Yang–Mills theory in which

- The leptons (electrons, neutrinos, . . .) and quarks are grouped into generations or families and
- They interact through the exchange of gauge bosons: the photon, W^+, W^-, and Z^0
- The masses of elementary particles in the field theory result from coupling to the *Higgs boson* H.
- The gauge bosons acquire finite masses without breaking gauge invariance (*spontaneous symmetry breaking*).

The particles of the Standard Model are listed in Table 8.3, along with their spins, charges, and masses (or experimental mass limits).

Table 8.3: Particles of the Standard Model

Particle	Symbol	Spin ($\hbar$)	Charge (e)	Mass (GeV c^{-2}) [†]
		— Leptons —		
Electron	e^-	$\frac{1}{2}$	-1	5.10999×10^{-4}
Electron neutrino	ν_e	$\frac{1}{2}$	0	$< 2 \times 10^{-9}$
Muon	μ^-	$\frac{1}{2}$	-1	0.10566
Muon neutrino	ν_μ	$\frac{1}{2}$	0	$< 1.9 \times 10^{-4}$
Tau	τ^-	$\frac{1}{2}$	-1	1.7841
Tau neutrino	ν_τ	$\frac{1}{2}$	0	$< 1.8 \times 10^{-2}$
		— Quarks —		
Down	d	$\frac{1}{2}$	$-\frac{1}{3}$	0.008
Up	u	$\frac{1}{2}$	$\frac{2}{3}$	0.004
Strange	s	$\frac{1}{2}$	$-\frac{1}{3}$	0.15
Charm	c	$\frac{1}{2}$	$\frac{2}{3}$	1.2
Bottom	b	$\frac{1}{2}$	$-\frac{1}{3}$	4.7
Top	t	$\frac{1}{2}$	$\frac{2}{3}$	175
		— Gauge and Higgs Bosons —		
Photon	γ	1	0	0
Charged weak bosons	$W^\pm$	1	± 1	81.0
Neutral weak boson	Z^0	1	0	92.4
Gluons	$G_1, G_2, \ldots, G_8$	1	0	0
Higgs	H	0	0	?
Graviton	g	2	0	0

[†]Quark masses are “current” or “Lagrangian” masses (the masses appearing in the field-theory Lagrangian). Effective masses inferred from quark models of hadrons are larger.

Table 8.4: Particle generations in the Standard Model

Generation	Leptons	Quarks	Quark mass scale (GeV)	Neutrino mass scale (GeV)
I	e^-, ν_e	d, u	0.006	$< 2 \times 10^{-9}$
II	μ^-, ν_μ	s, c	1	$< 1.9 \times 10^{-4}$
III	τ^-, ν_τ	b, t	100	$< 1.8 \times 10^{-2}$

- In the Standard Model, the matter fields are divided into three "generations" or "families", as illustrated in Table 8.4.
- An important ingredient of the Standard Model is that *the matter fields do not interact across family lines.*
- For the leptons this is implemented formally by assigning a lepton family number to each particle and requiring that interactions conserve this number.

Example: In Generation I

- Assign an electron family number of $+1$ to the electron and electron neutrino, -1 to the antielectron and the electron antineutrino, zero for all other particles.
- Then the reaction $\nu_e + n \rightarrow p + e^-$ conserves electron family number (because $1 + 0 = 0 + 1$) and is observed to occur.
- But the reaction $\nu_e + p \rightarrow n + e^+$ violates electron family number (because $1 + 0 \neq 0 + (-1)$) and has never been observed.

Generation	Leptons	Quarks	Quark mass scale (GeV)	Neutrino mass scale (GeV)
I	e^-, ν_e	d, u	0.006	$< 2 \times 10^{-9}$
II	μ^-, ν_μ	s, c	1	$< 1.9 \times 10^{-4}$
III	τ^-, ν_τ	b, t	100	$< 1.8 \times 10^{-2}$

- Also illustrated in the above table are characteristic mass scales for quarks and neutrinos within each generation.
- Neutrino masses are quoted as upper limits, since no neutrino mass has been measured directly thus far.
- The limits imply that *the neutrino masses are either zero or very tiny* on a mass scale set by the quarks of a generation.
- The explanation of this is a major unresolved issue in the theory of elementary particles.

In the Standard Model of elementary particle physics, it is *assumed* that the mass of all neutrinos is identically zero.

- The detailed justification of this statement requires quantum field theory somewhat beyond the scope of the present discussion.
- The central point is that there are potentially two kinds of neutrino mass terms that could appear in the theory:
  1. *Dirac masses*
  2. *Majorana masses.*
- The first is appropriate if the neutrino and antineutrino are separate particles.
- The second is appropriate if the neutrino is its own antiparticle (a possibility not ruled out by present experiment).
- *Both types of mass terms must vanish for Standard Model neutrinos,* but at least one could be non-zero in various extensions of the Standard Model.

8.8.1 Charged and Neutral Weak Currents

The Standard Model permits two basic kinds of weak interactions.

- In *charged weak currents* electrical charge is transferred in the interaction
  - The total charge is, of course, conserved.
  - Because charge is transferred, the boson mediating the force must be charged.
  - Thus, charged weak currents involve the W^+ and W^- weak gauge bosons.
- The uncharged weak gauge boson is the Z^0, and it can mediate *neutral weak currents* in which there is no transfer of charge in the weak interaction matrix elements.

A ν_e can interact with an electron through the charged weak current or the neutral weak current. However,

- A ν_μ or ν_τ cannot interact with an electron through exchange of a charged gauge boson without violating lepton family number conservation.
- Therefore, *only ν_e can undergo charged-current interactions with electrons.*

In contrast, *neutral current interactions can take place with any flavor of neutrino* without violating lepton family number conservation.

- Thus, electron neutrinos can interact with the electrons in normal matter through *both the charged and neutral weak currents.*
- All other flavors of neutrinos can interact with electrons *only through the neutral weak current.*

8.8.2 Mixing in the Quark Sector

The term *flavor* is used to distinguish the quarks and leptons of one generation from another.

- Thus, we shall often refer to ν_e, ν_μ, and ν_τ as different flavors of neutrinos, and to u, d, s, ... as different flavors of quarks.
- In the Standard Model, observations require that for quarks the mass eigenstates and the weak eigenstates are not equivalent.

  Thus, the quark states that enter the weak interactions are generally *linear combinations of the mass eigenstates.*

- Example: if we consider the first two generations, it is found that the d and s quarks enter the weak interactions in the "rotated" linear combinations d_c and s_c defined by the matrix equation

$$\begin{pmatrix} d_c \\ s_c \end{pmatrix} = \begin{pmatrix} \cos\theta_c & \sin\theta_c \\ -\sin\theta_c & \cos\theta_c \end{pmatrix} \begin{pmatrix} d \\ s \end{pmatrix}$$

  where d and s are the mass eigenstate quark fields and θ_c is termed the *mixing angle* or the *Cabibbo angle*.

- Comparison with data finds that the Cabbibo mixing angle is small:

$$\sin\theta_c \simeq 0.230 \qquad \cos\theta_c \simeq 0.973.$$

- In the more general case of three generations of quarks, weak eigenstates are described by a 3×3 mixing matrix called the *Cabibbo–Kobayashi–Maskawa or CKM matrix* that has *three real mixing angles and one phase.*

  There is little fundamental understanding of this quark flavor mixing, but the data clearly require it.

8.8.3 Mixing in the Leptonic Sector

Since in the Standard Model the quarks entering the weak interactions are mixtures of different mass eigenstates, we might expect that the corresponding leptons in these generations could also enter the weak interactions as mixed mass eigenstates.

- It is easy to show that if all flavors of neutrinos are identically massless (as is assumed in the Standard Model), the effect of a flavor mixing matrix has *no observable consequences.*
- However, if at least one neutrino has a non-zero mass, neutrino flavor mixing could have observable consequences.
- Conversely, observation of neutrino flavor mixing is a *direct indication that at least one neutrino has a finite mass.*

Thus either the observation of flavor oscillations, or directly of finite neutrino mass, would imply the existence of physics beyond the Standard Model.

8.9 Beyond the Standard Model: Finite Neutrino Masses

As noted above, a finite neutrino mass implies the possibility of flavor mixing for neutrinos.

- This would be of fundamental importance for elementary particle physics because it would imply new physics beyond the Standard Model.
- But it could be of equal importance for astrophysics because it provides a possible solution of the solar neutrino problem:
  - As we shall show below, if neutrino flavor eigenstates are mixtures of mass eigenstates, neutrinos propagating in time will oscillate in flavor.
  - If neutrino flavors can oscillate, then it is possible that when some of the electron neutrinos emitted by the Sun reach Earth they would have oscillated into another flavor.
  - Since the experiments described earlier are sensitive only to electron neutrinos, they would miss any neutrinos that had oscillated into other flavors, thus (possibly) explaining the observed neutrino deficit.

Standard Model neutrinos *must* be massless.

- However, there are many reasons to believe that the Standard Model—despite its remarkable success—is incomplete and represents a low-energy approximation to a more complete theory.
  - There are more than 20 adjustable parameters that have no convincing fundamental constraint.
  - The origin of mass through the Higgs mechanism is purely phenomenological.
  - The generational (family) structure is based entirely on phenomenology.
  - Violations of symmetries such as parity are put by hand, . . .
- Various extensions such as *Grand Unified Theories (GUTs)* have been proposed that go beyond the Standard Model.
- For these theories often the reasons that mass terms are forbidden in the Standard Model are not operative and *neutrino mass terms may occur naturally.*

We must entertain the possibility of physics beyond the Standard Model and thus of finite neutrino masses.

8.10 Neutrino Vacuum Oscillations

The preceding discussion suggests that neither direct experimental measurement, nor fundamental principle, nor our present understanding of the Standard Model extended to Grand Unified Theories preclude a small mass for neutrinos. Therefore, let us pursue the possibility that

- Finite-mass neutrinos undergo flavor oscillations.
- These oscillations could account for the solar neutrino deficit.

8.10.1 Mixing for Two Neutrino Flavors

Let us first consider neutrino oscillations in a two-flavor model, in the absence of matter. *(Note: $\hbar = c = 1$ units; see Appendix B.2.)*

- We shall term these *vacuum oscillations* and use a subscript v to distinguish them from oscillations that occur in the presence of matter.
- Generally, we shall use $\theta_{\rm v}$ to denote neutrino vacuum oscillation angles and $\theta_{\rm m}$ to denote oscillation angles in matter.
- We shall sometimes use θ to denote either if it is clear from the context which is meant.
- The flavor eigenstates $\nu_{\rm e}$ and ν_μ may be expressed in terms of the mass eigenstates ν_1 and ν_2 through the matrix transformation

$$\underbrace{\begin{pmatrix} \nu_{\rm e} \\ \nu_\mu \end{pmatrix}}_{\text{flavor eigenstates}} = \underbrace{\begin{pmatrix} \cos\theta_{\rm v} & \sin\theta_{\rm v} \\ -\sin\theta_{\rm v} & \cos\theta_{\rm v} \end{pmatrix}}_{\text{flavor mixing matrix}} \underbrace{\begin{pmatrix} \nu_1 \\ \nu_2 \end{pmatrix}}_{\text{mass eigenstates}} ,$$

  where $\theta_{\rm v}$ is the (phenomenological) *vacuum mixing angle.* Thus,

$$|\nu_{\rm e}\rangle = \cos\theta_{\rm v}|\nu_1\rangle + \sin\theta_{\rm v}|\nu_2\rangle \qquad |\nu_\mu\rangle = -\sin\theta_{\rm v}|\nu_1\rangle + \cos\theta_{\rm v}|\nu_2\rangle .$$

- The mass eigenstates may in turn be expressed as a linear combination of the flavor eigenstates (see Exercise):

$$\begin{pmatrix} \nu_1 \\ \nu_2 \end{pmatrix} = \begin{pmatrix} \cos\theta_{\rm v} & -\sin\theta_{\rm v} \\ \sin\theta_{\rm v} & \cos\theta_{\rm v} \end{pmatrix} \begin{pmatrix} \nu_{\rm e} \\ \nu_\mu \end{pmatrix} .$$

- Assuming that at least one of the neutrino masses is non-zero, the different mass eigenstates will move with slightly different speeds as neutrinos propagate in time.
- Thus, the expansion coefficients in the above equation will vary with time and the probability of detecting a particular flavor of neutrino will oscillate with time, or equivalently, with the distance traveled.
- From basic quantum mechanics the *mass eigenstates* evolve with time t according to

$$|\nu_i(t)\rangle = e^{-iE_i t}|\nu_i(0)\rangle,$$

  where the index i labels mass eigenstates of energy E_i.
- Thus the time evolution of the ν_e state will be given by

$$\begin{aligned}|\nu(t)\rangle &= \cos\theta_v|\nu_1(t)\rangle + \sin\theta_v|\nu_2(t)\rangle \\ &= \cos\theta_v e^{-iE_1 t}|\nu_1(0)\rangle + \sin\theta_v e^{-iE_2 t}|\nu_2(0)\rangle,\end{aligned}$$

  and this may be expressed as the mixed-flavor state (see Exercise)

$$\begin{aligned}|\nu(t)\rangle = (&\cos^2\theta_v e^{-iE_1 t} + \sin^2\theta_v e^{-iE_2 t})|\nu_e\rangle \\ &+ \sin\theta_v\cos\theta_v(-e^{-iE_1 t} + e^{-iE_2 t})|\nu_\mu\rangle.\end{aligned}$$

- We see that the mixed flavor state

$$|\nu(t)\rangle = (\cos^2\theta_v e^{-iE_1 t} + \sin^2\theta_v e^{-iE_2 t})|\nu_e\rangle + \sin\theta_v\cos\theta_v(-e^{-iE_1 t} + e^{-iE_2 t})|\nu_\mu\rangle.$$

starts out as pure ν_e at $t = 0$,

$$|\nu(0)\rangle = \underbrace{(\cos^2\theta_v + \sin^2\theta_v)}_{=1}|\nu_e\rangle + \underbrace{\sin\theta_v\cos\theta_v(-1+1)}_{=0}|\nu_\mu\rangle = |\nu_e\rangle,$$

but will be mixed ν_e and ν_μ after a finite time.

- Taking the overlap of

$$|\nu(t)\rangle = (\cos^2\theta_v e^{-iE_1 t} + \sin^2\theta_v e^{-iE_2 t})|\nu_e\rangle + \sin\theta_v\cos\theta_v(-e^{-iE_1 t} + e^{-iE_2 t})|\nu_\mu\rangle.$$

with the flavor eigenstates, we find that the probabilities for an initial electron neutrino flavor state to remain an electron neutrino, or be converted to a muon neutrino after a time t, are given by

$$\begin{aligned} P(\nu_e \to \nu_e, t) &= |\langle\nu_e|\nu(t)\rangle|^2 \\ &= 1 - \tfrac{1}{2}\sin^2(2\theta_v)[1 - \cos(E_2 - E_1)t] \quad \text{(remain } \nu_e\text{)} \\ P(\nu_e \to \nu_\mu, t) &= |\langle\nu_\mu|\nu(t)\rangle|^2 \\ &= \tfrac{1}{2}\sin^2(2\theta_v)[1 - \cos(E_2 - E_1)t] \quad \text{(become } \nu_\mu\text{)}. \end{aligned}$$

with the sum of probabilities equal to unity.

8.10.2 The Vacuum Oscillation Length

- If we assume that the two energies E_1 and E_2 are approximately equal and much larger than mc^2 for the neutrino masses,

$$E_i = (p^2 + \underbrace{m_i^2}_{\text{small}})^{1/2} \simeq p + \frac{m_i^2}{2p}, \quad \longrightarrow \quad E_2 - E_1 \simeq \frac{\Delta m^2}{2E}$$

  where $E_1 \sim E_2 \equiv E$ and

$$\Delta m^2 \equiv m_2^2 - m_1^2.$$

- The probability for flavor survival and conversion as a function of distance traveled $r \sim ct$ may then be expressed as (see Exercise)

$$P(\nu_e \to \nu_e, r) = 1 - \sin^2(2\theta_v)\sin^2\left(\frac{\pi r}{L}\right)$$
$$P(\nu_e \to \nu_\mu, r) = \sin^2(2\theta_v)\sin^2\left(\frac{\pi r}{L}\right),$$

  where θ_v is the mixing angle and the *oscillation length* L is defined by

$$L \equiv \frac{4\pi E}{\Delta m^2}.$$

  Physically L is the distance required, assuming $v \simeq c$, for one one complete flavor oscillation (for example, $\nu_e \to \nu_\mu \to \nu_e$).

- Restoring the factors of $\hbar$ and c in the preceding equation

$$L = \frac{4\pi E\hbar}{\Delta m^2 c^3} = 2.48\left(\frac{E}{\text{MeV}}\right)\left(\frac{\text{eV}^2}{\Delta m^2}\right),$$

  where L is in meters, the neutrino energy E is in MeV, and the mass squared difference Δm^2 is in eV.

8.11 Oscillations in Matter: The MSW Effect

The vacuum neutrino oscillations described in the previous section could in principle account for the depressed flux of solar neutrinos detected on Earth.

- But such a solution requires a *relatively large value of the mixing angle* in order to suppress the electron neutrino flux sufficiently.
- Because the *quark-sector mixing angles are relatively small,* theoretical prejudice (but no very solid evidence) initially favored a small mixing angle in the neutrino sector also.
- However, there is another issue that we have not yet addressed: *the neutrinos also have to transit out of the Sun.*
- *Electron neutrinos couple more strongly to normal matter than do other neutrinos* (because electron neutrinos and the particles making up normal matter all reside in the first generation of the Standard Model).
- Thus we must also ask how interaction with solar material will influence neutrino oscillations.

8.11.1 The Mass Matrix

Let us first introduce an alternative formulation of the neutrino vacuum oscillation problem.

- Again taking two-neutrino mixing for simplicity, a neutrino in a momentum state p propagating in the vacuum can be written as a time-dependent linear combination of flavor eigenstates

$$|\nu(t)\rangle = \nu_e(t)|\nu_e\rangle + \nu_\mu(t)|\nu_\mu\rangle,$$

  where the time-dependent amplitudes $\nu_e(t)$ and $\nu_\mu(t)$ obey the matrix equation

$$i\frac{d}{dt}\begin{pmatrix} \nu_e(t) \\ \nu_\mu(t) \end{pmatrix} = M_0 \begin{pmatrix} \nu_e(t) \\ \nu_\mu(t) \end{pmatrix}.$$

- The mass matrix in vacuum, M_0, is given by

$$M_0 = \begin{pmatrix} E_1\cos^2\theta + E_2\sin^2\theta & (E_2 - E_1)\sin\theta\cos\theta \\ (E_1 - E_2)\sin\theta\cos\theta & E_1\sin^2\theta + E_2\cos^2\theta \end{pmatrix},$$

  where θ is the mixing angle and

$$E_i = (p^2 + m_i^2)^{1/2} \simeq p + \frac{m_i^2}{2p},$$

  assuming that $E_i >> m_i c^2$.

- After subtracting a multiple of the unit matrix (which will not influence the flavor probabilities), the vacuum mass matrix can be cast in the form

$$M_0 = \frac{\pi}{L}\begin{pmatrix} \cos 2\theta & -\sin 2\theta \\ -\sin 2\theta & -\cos 2\theta \end{pmatrix},$$

  where L is the vacuum oscillation length introduced earlier.

8.11.2 Propagation of Neutrinos in Matter

So far, this is just a reformulation of our previous equations for vacuum oscillation.

- Now, following the insight of *Mikheyev, Smirnov, and Wolfenstein (MSW),* we consider the additional influence that interaction with matter may have on the neutrino oscillation.
- When electron neutrinos scatter elastically from electrons in the Sun, they may do so through either the charged weak current or the neutral weak current.

Box 8.1 Feynman Diagrams

In quantum field theory we use a pictorial representation of interaction matrix elements called *Feynman diagrams.*

- They are highly intuitive: given a Feynman diagram one can write the corresponding matrix element and given the matrix element one can sketch the Feynman diagram.
- Here are some weak-interaction Feynman diagrams:

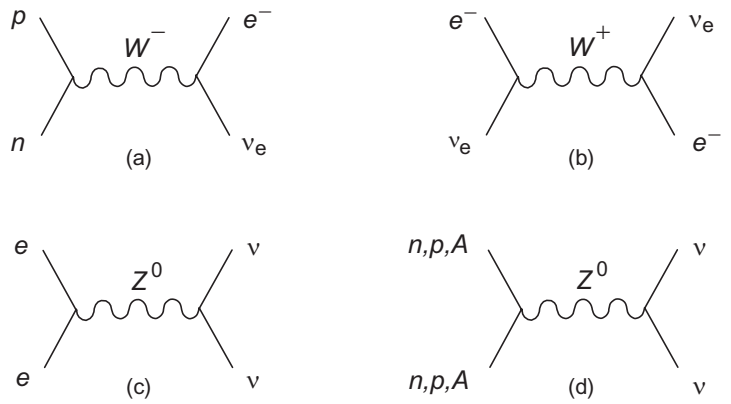

- The solid lines represent (fermion) matter fields and the wiggly lines represent exchanged virtual gauge bosons.
- Each diagram can represent several related processes, depending on the direction in which it is read.
- For example, diagram (a) read from the bottom:
  1. A neutron (n) exchanges a virtual W^- intermediate vector boson with an electron neutrino (ν_e).
  2. This converts $n \rightarrow p$ and $\nu \rightarrow e^-$.
- Absence of flavor indices on neutrinos in diagrams (c) and (d) indicates that *the neutral current is flavor blind.* The symbol A in diagram (d) stands for a composite nucleus.

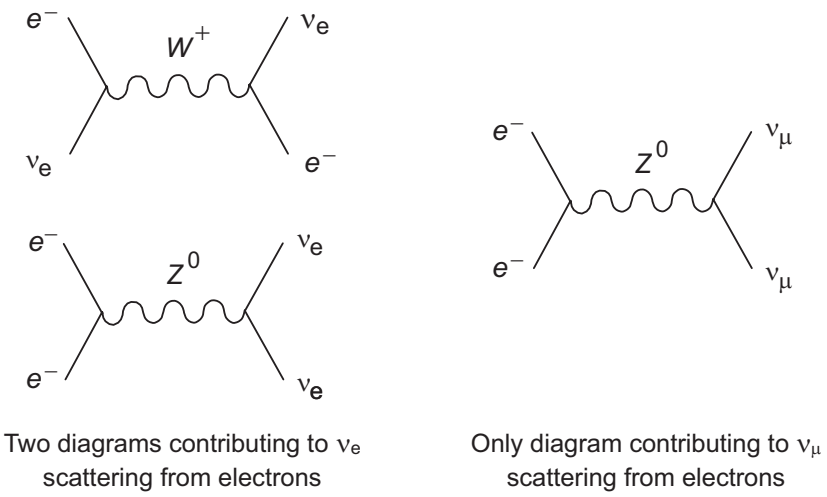

Figure 8.7: Feynman diagrams responsible for neutrino–electron scattering in the MSW effect.

Figure 8.7 illustrates Feynman diagrams relevant to neutrino scattering in the Sun.

- Both the neutral and charged current contribute to electron neutrino interactions (left two diagrams).
- Only the neutral current contributes to the muon neutrino interactions.
- Neutral current contributes to both ν_e and ν_μ scattering, so neglect this common contribution for this discussion.
- Vacuum neutrino oscillations will be modified in matter because of the charged-current (W^+) diagram in Fig. 8.7 contributing to ν_e scattering but not to ν_μ.

The situation is similar to two coupled oscillators where the frequency of one oscillator is modified more by coupling to its surroundings than the other. Such a modification will influence the nature of the coupling between the two oscillators.

- The charged-current Feynman diagram contributes an additional term to the vacuum-scattering mass matrix that may be expressed as

$$M' = \sqrt{2} G_{\mathrm{F}} n_{\mathrm{e}} |\nu_{\mathrm{e}}\rangle\langle\nu_{\mathrm{e}}|,$$

  where G_{F} is the weak coupling constant, n_{e} is the local electron number density,

- $|\nu_{\mathrm{e}}\rangle\langle\nu_{\mathrm{e}}|$ is a *projection operator* that selects the electron neutrino eigenstate (it causes M' applied to a wavefunction to give zero unless that wavefunction corresponds to a ν_{e} eigenstate).

- With this additional contribution, the mass matrix in the presence of matter becomes

$$M = \frac{\pi}{L} \begin{pmatrix} \cos 2\theta + L/\ell_{\mathrm{m}} & -\sin 2\theta \\ -\sin 2\theta & -\cos 2\theta - L/\ell_{\mathrm{m}} \end{pmatrix}.$$

- The additional matter contribution to the oscillation length ℓ_{m} is given by

$$\ell_{\mathrm{m}} = \frac{\sqrt{2}\pi}{G_{\mathrm{F}} n_{\mathrm{e}}} = \frac{1.77 \times 10^{7}}{\rho_{\mathrm{e}}} \text{ meters}$$

  where ρ_{e} is the electron number density in units of Avogadro's number per cm^{-3}.

- The time-evolved states in matter, $|\nu_1^{\rm m}\rangle$ and $|\nu_2^{\rm m}\rangle$, may be obtained by diagonalizing

$$M = \frac{\pi}{L}\begin{pmatrix} \cos 2\theta + L/\ell_{\rm m} & -\sin 2\theta \\ -\sin 2\theta & -\cos 2\theta - L/\ell_{\rm m} \end{pmatrix}.$$

- Then the electron neutrino state after a time t becomes

$$\begin{aligned} |\nu(t)\rangle = (&\cos^2\theta_{\rm m} e^{-iE_1 t} + \sin^2\theta_{\rm m} e^{-iE_2 t})|\nu_{\rm e}\rangle \\ &+ \sin\theta_{\rm m}\cos\theta_{\rm m}(-e^{-iE_1 t} + e^{-iE_2 t})|\nu_\mu\rangle, \end{aligned}$$

  which is analogous to the corresponding vacuum equation, but

- The vacuum mixing angle $\theta_{\rm v}$ is replaced by the matter mixing angle $\theta_{\rm m}$,

$$\tan 2\theta_{\rm m} = \frac{\sin 2\theta_{\rm v}}{\cos 2\theta_{\rm v} \pm L/\ell_{\rm m}}$$

  (with $+$ for $m_1 > m_2$ and $-$ for $m_1 < m_2$),

- The vacuum oscillation length L is replaced by the oscillation length in matter

$$L_{\rm m} = \frac{L}{\sqrt{1 + \dfrac{2L}{\ell_{\rm m}}\cos 2\theta_{\rm v} + \dfrac{L^2}{\ell_{\rm m}^2}}}.$$

- For a fixed $n_{\rm e}$, the flavor probabilities are given by the vacuum equations with the replacements $\theta_{\rm v} \to \theta_{\rm m}$ and $L \to L_{\rm m}$.

$$P(\nu_{\rm e} \to \nu_{\rm e}, r) = 1 - \sin^2(2\theta_{\rm m})\sin^2(\pi r/L_{\rm m})$$

$$P(\nu_{\rm e} \to \nu_\mu, r) = \sin^2(2\theta_{\rm m})\sin^2(\pi r/L_{\rm m}).$$

- Generally, $\theta_{\rm m}$ and $L_{\rm m}$ will vary with the solar depth since they depend on the number density $n_{\rm e}$.

8.11.3 The MSW Resonance Condition

- From

$$P(\nu_e \to \nu_e, r) = 1 - \sin^2(2\theta_m)\sin^2(\pi r/L_m)$$
$$P(\nu_e \to \nu_\mu, r) = \sin^2(2\theta_m)\sin^2(\pi r/L_m).$$

  we see that *maximal flavor mixing* occurs when $\sin^2(2\theta_m) = 1$ or $\theta_m = \frac{\pi}{4}$.

- The most significant property of

$$\tan 2\theta_m = \frac{\sin 2\theta_v}{\cos 2\theta_v \pm L/\ell_m}$$

  relative to the vacuum solution is that if Δm^2 and L are positive (which requires that $m_1 < m_2$ and selects the negative sign in the above equation),

$$\theta_m \to \frac{\pi}{4} \quad \text{and} \quad \tan 2\theta_m \to \infty \quad \text{when} \quad \cos 2\theta_v = \frac{L}{\ell_m},$$

- Because

$$\ell_m = \frac{\sqrt{2}\pi}{G_F n_e} \qquad L = \frac{4\pi E}{\Delta m^2},$$

  this occurs when the electron density satisfies

$$n_e = \frac{\cos 2\theta_v \Delta m^2}{2\sqrt{2} G_F p} \equiv n_e^R.$$

- From

$$P(\nu_e \to \nu_e, r) = 1 - \sin^2(2\theta_m)\sin^2(\pi r/L_m)$$
$$P(\nu_e \to \nu_\mu, r) = \sin^2(2\theta_m)\sin^2(\pi r/L_m).$$

$\theta_m \to \frac{\pi}{4}$ corresponds to a *resonance condition* leading to maximal mixing between ν_e and ν_μ, with a survival probability

$$P(\nu_e \to \nu_e, r) = 1 - \sin^2\left(\frac{\pi r}{L_m}\right) \qquad \text{(Resonance)},$$

and an oscillation length

$$L_m = \frac{L}{\sin 2\theta_v} \qquad \text{(Resonance)}.$$

- This is the *Mikheyev–Smirnov–Wolfenstein* or *MSW resonance*.

> *No matter how small the vacuum mixing angle θ_v, as long as it is not zero there is some value of the electron density n_e^R where the MSW resonance condition occurs and one obtains maximal flavor mixing at that density.*

- Note that if the mixing angle θ_v is small the corresponding oscillation length

$$L_m = \frac{L}{\sin 2\theta_v}.$$

will be large.

If the condition $m_1 < m_2$ is not satisfied there is no resonance for electron neutrinos because then the positive sign would be chosen in

$$\tan 2\theta_{\mathrm{m}} = \frac{\sin 2\theta_{\mathrm{v}}}{\cos 2\theta_{\mathrm{v}} \pm L/\ell_{\mathrm{m}}}$$

and the denominator will not go to zero. In that case one can show that there is a corresponding resonance condition instead for the electron antineutrino $\overline{\nu}_{\mathrm{e}}$. This would be very interesting physics but could not be used to solve the problem of an observed deficit of solar ν_{e} in detectors on Earth.

8.11.4 Resonance Flavor Conversion

- If, for example,
  - $m_1 < m_2$ and θ_v is small so that $|\nu_e\rangle \simeq |\nu_1^m\rangle$, and
  - the electron density in the central part of the Sun where the neutrino is produced satisfies $n_e > n_e^R$,

  a neutrino leaving the Sun will inevitably encounter the MSW resonance while on its way out of the Sun.
- If the change in density is sufficiently slow (adiabatic condition), the ν_e flux produced in the core can be almost entirely converted to ν_μ by the MSW resonance near the radius where the resonance condition is satisfied.

The MSW resonance conversion of flavors can be viewed as an adiabatic level crossing

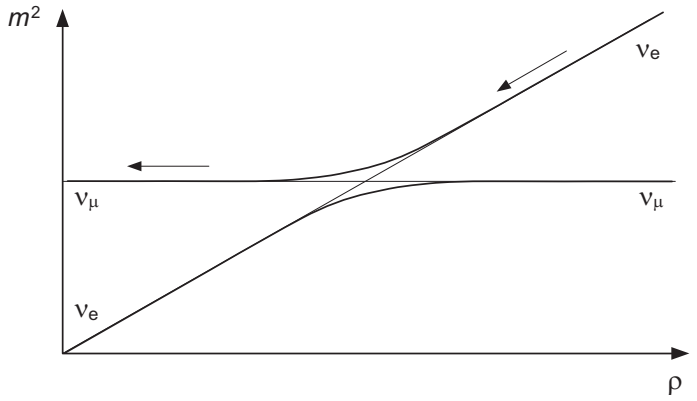

- If the level crossing is adiabatic, a neutrino that starts out near the center as a ν_e (corresponding to high density on the right side of the figure) changes adiabatically into a ν_μ by the time it exits the Sun (corresponding to low density in the left side of the figure).
- That is, the neutrino follows the upper curved trajectory though the resonance in the level-crossing region, as indicated by the arrows.

Therefore, the neutrino can emerge from the Sun in a completely different flavor state than the one in which it was created.

8.12 Resolution of the Solar Neutrino Problem

A series of experiments have in principle resolved the solar neutrino problem.

- These experiments demonstrate rather directly that flavor conversion of neutrinos is taking place.
- This, in turn then implies that at least some neutrinos have mass.
- Detailed comparison of these experiments indicates that solar electron neutrinos are being converted to muon neutrinos by neutrino oscillations,
- If all flavors of neutrinos coming from the Sun are detected the solar neutrino deficit relative to the Standard Solar Model disappears.
- The favored oscillation scenario is MSW resonance conversion in the Sun, but for a *large vacuum mixing angle solution.*

Let us now describe briefly the experiments that have led to these rather remarkable conclusions.

8.12.1 Super Kamiokande Observation of Flavor Oscillation

The Super Kamiokande detector has been used to observe neutrinos produced in atmospheric cosmic ray showers.

- When high-energy cosmic rays hit the atmosphere, they generate showers of mesons that decay to muons, electrons, positrons, and neutrinos.
- Theory assuming no physics beyond the Standard Model indicates that the ratio of muon neutrinos plus antineutrinos to electron neutrinos plus antineutrinos should be 2,

$$R \equiv \frac{\nu_\mu + \bar{\nu}_\mu}{\nu_e + \bar{\nu}_e} = 2 \qquad \text{(Standard Model)}.$$

- Instead, Super Kamiokande confirmed that the ratio R is only 64% of what is expected.
- This result could be explained by neutrino flavor oscillations: if, for example, the muon neutrinos oscillate into another flavor, the observed ratio would be reduced below the expected value.

Attribution of the anomalous ratio found for

$$R \equiv \frac{\nu_\mu + \bar{\nu}_\mu}{\nu_e + \bar{\nu}_e} = 2 \qquad \text{(Standard Model)}.$$

to a flavor oscillation was strengthened by the observed dependence of the ratio R for higher-energy neutrinos on the zenith angle φ for the neutrinos.

- This observation is possible because the water Čerenkov detectors give directional information on the detected neutrinos.
- Detailed observations indicated that for muon neutrinos of the highest energy,
  - $R \simeq 1$ for neutrinos coming directly up through the Earth and into the detector ($\varphi = 180^\circ$) but
  - $R \simeq 2$ for those neutrinos coming from directly overhead ($\varphi = 0^\circ$).
- Similar measurements for electron neutrinos indicated no such asymmetry.

- These results can be explained by oscillations of the muon neutrino because the zenith angle is a measure of how far the neutrino has traveled since it was produced in the atmosphere.
  - Atmospherically-produced neutrinos coming up through the Earth have traveled more than the diameter of the Earth since they were produced in an atmospheric shower on the opposite side of the Earth
  - Neutrinos coming from a shower directly overhead have traveled a distance that is only a fraction of the height of the atmosphere.
- If the oscillation length L is less than the diameter of the Earth but greater than the height of the atmosphere, neutrinos coming from below the detector would be strongly influenced by oscillation but those coming from directly overhead would have little chance to oscillate into another flavor before being detected.

Detailed analysis suggests that the oscillation partner of the muon neutrino is not the electron neutrino

- Hence these results are not directly applicable to the solar neutrino problem.
- ν_μ is oscillating either with the tau neutrino or some other flavor of neutrino that does not undergo normal weak interactions but does participate in neutrino oscillations (‘ sterile neutrinos”).
- The best fit to the data suggests a mixing angle close to maximal (a *large mixing angle solution*) and a mass squared difference in the range

$$\Delta m^2 \simeq 5 \times 10^{-4} - 6 \times 10^{-3}\ \mathrm{eV}^2.$$

- The large mixing angle indicates that the mass eigenstates are approximately equal mixtures of the two weak flavor eigenstates.

8.12.2 SNO Observation of Neutral Current Interactions

The Super Kamiokande results cited above indicate conclusively the existence of neutrino oscillations and thus of physics beyond the Standard Model.

- However, the detected oscillations do not appear to involve the electron neutrino.
- Thus the Super Kamiokande results cannot be applied directly to the solar neutrino problem.

But a water Čerenkov detector in Canada has yielded information about neutrino oscillations that *is* directly applicable to the solar neutrino problem.

The Sudbury Neutrino Observatory (SNO) differs from Super-K in that it contains heavy water

- The heavy water is important because of the deuterium that it contains.
- In regular water, to produce sufficient Čerenkov light the ν energy has to be greater than about 5–7 MeV.
- Because deuterium (d) contains a weakly-bound neutron, it can undergo a breakup reaction:
  - Any flavor neutrino can initiate the reaction

$$\nu + d \rightarrow \nu + p + n \qquad \text{(Neutral current)},$$

  - but only electron neutrinos can initiate

$$\nu_e + d \rightarrow e^- + p + p \qquad \text{(Charged current)}.$$

- Both of these reactions have much larger cross sections than elastic neutrino–electron scattering, so SNO can gather events at relatively high rates.
- The energy threshold can be lowered to 2.2 MeV, the binding energy of the deuteron.
- Because the neutral currents are flavor blind, $\nu + d \rightarrow \nu + p + n$ gives SNO the ability to see the *total neutrino flux of all flavors* coming from the Sun.

Table 8.5: Comparison of SNO results and Standard Solar Model predictions for solar neutrino fluxes. All fluxes are in units of 10^6 cm^2 s^{-1}.

SSM ν_e Flux	SNO ν_e Flux	SNO ν_e/SSM	SNO all flavors	SNO All/ SSM
5.05 ± 0.91	1.76 ± 0.11	0.348	5.09 ± 0.62	1.01

Because of its energy threshold, SNO sees primarily ^{8}B solar neutrinos.

- The initial SNO results confirmed results from the pioneering solar neutrino experiments: a strong suppression of the electron neutrino flux is observed relative to that expected in the Standard Solar Model.
- Specifically, SNO found that only about $\frac{1}{3}$ of the expected ν_e were being detected.

However, SNO went further.

- By analyzing the flavor-blind weak neutral current events, it was possible to show that

  > The total flux of *all neutrinos* in the detector was almost exactly that expected from the Standard Solar Model.

- Table 8.5 summarizes.

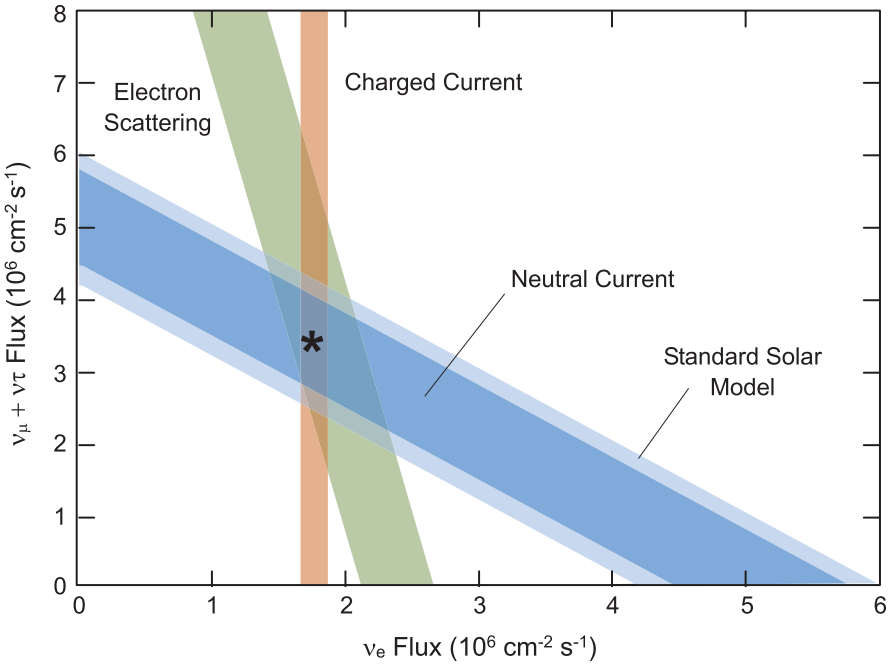

Figure 8.8: Flux of neutrinos from ^{8}B in the Sun detected for various flavors by SNO. Bands represent one standard deviation for each class of reaction. Best overall fit is indicated by the star and suggests that $\frac{2}{3}$ of the Sun's ^{8}B neutrinos have changed flavor between being the core of the Sun and the Earth. The Standard Solar Model band is the prediction for the ^{8}B flux, irrespective of flavor changes.

The SNO case for neutrino oscillation was strengthened by analysis of neutrino–electron elastic scattering data (largely from Super K) combined with SNO data from

$$\nu_e + d \rightarrow e^- + p + p \qquad \text{(Charged current)}.$$

which estimates the total neutrino flux of all flavors.

- Figure 8.8 illustrates.
- The best fit indicates that $\frac{2}{3}$ of the Sun's electron neutrinos have changed flavor when they reach the Earth.

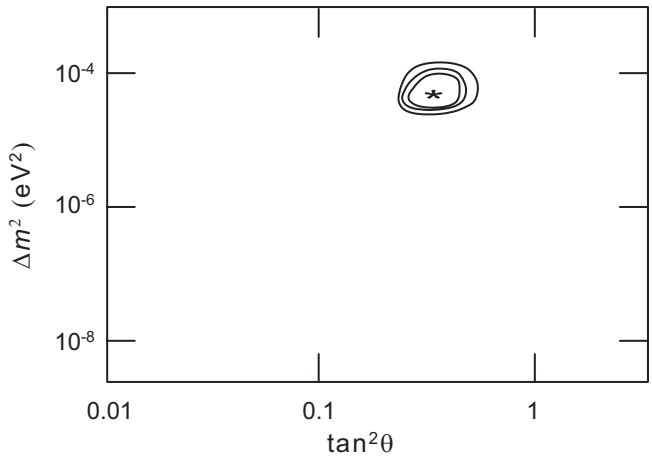

Figure 8.9: Two-flavor neutrino oscillation parameters from SNO. Shown are the 99%, 95% and 90% confidence contours, with the star at the most likely value.

Assuming a two-flavor mixing model, it is common to plot confidence level contours in a two dimensional plane with Δm^2 on one axis and $\tan^2\theta$ on the other.

- Figure 8.9 shows the best-fit confidence-level contours for parameters based on current SNO data.
- The SNO results suggest that the solar neutrino problem is solved by neutrino oscillations between ν_e and ν_μ flavors, with parameters

$$\Delta m^2 \sim 10^{-4}\ \text{eV}^2 \qquad \theta \simeq 30^\circ.$$

- This is again a large-mixing-angle solution, which implies that a ν_e is actually almost an equal superposition of two mass eigenstates, probably separated by no more than a few hundredths of an eV.

8.12.3 KamLAND Constraints on Mixing Angles

KamLAND is housed in the same Japanese mine cavern that housed Kamiokande, predecessor to Super-K.

- It uses phototubes to monitor a large container of liquid scintillator.
- It looks specifically for electron antineutrinos produced during nuclear power generation in a set of 22 Japanese and Korean reactors that are located within a few hundred kilometers of the detector.
- The antineutrinos are detected from the inverse β-decay in the scintillator:

$$\bar{\nu}_e + p \rightarrow e^+ + n.$$

- From power levels in the reactors, the expected antineutrino flux at KamLAND can be modeled.
- The experiment has detected a shortfall of antineutrinos, consistent with a large-angle neutrino oscillation solution having

$$\Delta m^2 = 6.9 \times 10^{-5}\ \text{eV}^2 \qquad \theta = 45^\circ.$$

- KamLAND results exclude at the 95% level all previously proposed alternatives to a large-angle solution.

The SNO and KamLAND results together greatly shrink the allowed parameter space for solar neutrino oscillation parameters.

- The large mixing angle solutions implied by SNO and KamLAND for the ν_e–ν_μ mixing indicate that the vacuum oscillations of solar neutrinos are of secondary importance to the MSW matter oscillations in the body of the Sun itself.
- Because the inferred vacuum oscillation lengths for the large-angle solutions are much less than the Earth–Sun distance, they would largely wash out any energy dependence of the neutrino shortfall.
- Since the detectors indicate that such an energy dependence exists, *the MSW resonance is strongly implicated as the source of the neutrino flavor conversion responsible for the "solar neutrino problem".*

Ironically, the MSW effect was proposed to justify a small mixing angle solution but instead seems to resolve the solar neutrino anomaly through a large mixing angle solution.